Temperature Error Correction Based on BP Neural Network in Meteorological Wireless Sensor Network

Baowei Wang[1,2,3(✉)], Xiaodu Gu[1,3], Li Ma[1,3,4], and Shuangshuang Yan[1,3]

[1] School of Computer and Software, Nanjing University of Information Science and Technology, Nanjing 210044, China
wbw.first@163.com,1398499567@qq.com

[2] Jiangsu Collaborative Innovation Center on Atmospheric Environment and Equipment Technology, Nanjing 210044, China

[3] Jiangsu Engineering Center of Network Monitoring, Nanjing University of Information Science and Technology, Nanjing 210044, China
hotyss@hotmail.com

[4] Key Laboratory of Meteorological Disaster of Ministry of Education, Nanjing University of Information Science and Technology, Nanjing 210044, China
mali1775088@163.com

Abstract. Using meteorological wireless sensor network to monitor the air temperature (AT) can greatly reduce the costs of monitoring. And it has the characteristics of easy deployment and high mobility. But low cost sensor is easily affected by external environment, often lead to inaccurate measurements. Previous research has shown that there is a close relationship between AT and solar radiation (SR). Therefore, We designed a back propagation (BP) neural network model using SR as the input parameter to establish the relationship between SR and AT error (ATE) with all the data in May. Then we used the trained BP model to correct the errors in other months. We evaluated the performance on the data sets in previous research and then compare the maximum absolute error, mean absolute Error and standard deviation respectively. The experimental results show that our method achieves competitive performance. It proves that BP neural network is very suitable for solving this problem due to its powerful functions of non-linear fitting.

Keywords: Wireless sensor network · Data correction · Artificial neural network · Solar radiation

1 Introduction

Meteorological parameter monitoring [27] is not only the base of weather forecast, climate prediction, scientific research, and the foundation of other kinds of meteorological services, but also the impetus of the development of Meteorological Science [16]. In the past many years, China affected by meteorological disasters seriously. In order to effectively reduce the meteorological disasters

X. Sun et al. (Eds.): ICCCS 2016, Part II, LNCS 10040, pp. 117–132, 2016.
DOI: 10.1007/978-3-319-48674-1_11

caused economic losses, we urgently need a comprehensive, three-dimensional, continuous observation to the meteorological data to improve the monitoring accuracy.

At present, meteorological data monitoring in China mainly depends on the nationwide automatic weather station(AWS) [4,18]. Wide application of the automatic weather station has greatly improved the development of meteorological services. But there are still many deficiencies in the current observation mode: the site distribution of low density, location poor mobility, high cost and so on. Secondly, the deployment of automatic weather station is too single and the meteorological elements sensor deployment is too concentrated, it is difficult to ensure the best observation position. Finally, the current automatic weather station has the characteristic of poor mobility, high cost and long period. It is difficult to meet emergencies or natural disasters emergency encryption meteorological monitoring needs.

The application of wireless sensor network (WSN) [21,24,29] in meteorological observation and the formation of meteorological sensor network has many significant advantages. Firstly, the wireless communication technology makes the meteorological data no longer rely solely on the cable transmission, making deployment and data collection of meteorological sensors become more convenient, so as to enhance the emergency handling ability. Secondly, using a large number of sensor nodes and collect meteorological data, and results are obtained through the fusion processing [15] are more accurate than obtained by single sensor observation. It can also avoid the problem of deployed in a single location and easily affected by accidental factors. However, the professional meteorological sensor node is expensive and can not meet the large deployment requirements. Thus, many researchers are looking into the low price of the on-board sensors or non professional meteorological sensors, and use data fusion [12,20], data correction method to compensate the defect of low accuracy, in order to improve the measurement accuracy. This paper use the on-board temperature sensor for meteorological data collection, then the use of artificial intelligence algorithm [5,22,23] to correct the sampling data to improve the accuracy of meteorological sensor network data.

In this paper, we use the advantages of WSNs to collect the data of AT and other parameters. The sensor nodes were deployed in the university campus and automatic weather station nearby. In addition, our sensing node can be connected with specialized meteorological sensors. However, the cost still large if we apply specialized temperature sensor on every node. Thus, we use on-board temperature sensor. The sensor embedded in our nodes is SHT15 [1,2] which can collect humidity and temperature data and whose cost ranges from only 3 to 10 dollars. Comparing to the specialized meteorological sensor HMP45D [7,13], SHT15 is very cheap.

However, the accuracy of SHT15 is easily affected by external environment, often lead to inaccurate measurements. Many researchers are trying to improve the accuracy by using data fusion, data correction method to compensate the defect of low accuracy. So, this is also the work we want to do. Previous studies

show that AT [14,28] is affected by SR [3,17] best. And our low cost sensor is affected by SR most seriously. So, it is reasonable for us to take SR into account in this work to correct the AT error (ATE).

Since there is a close relationship between ATE and SR, The most important thing is to find a method or formula to establish the relationship between them. But we can not find a precise formula to calculate the ATE of every SR. An existing work in [16] has given a approach using BP neural network to reduce the errors in sensing data. But they did not take the SR into account. This method needs to establish many BP models for each weather condition. And even in the same weather conditions, it also has to establish all kinds of BP models for different months. This method not only needs a lot of work, but also the effect of the correction is not very good. An other existing work on the improvement of the accuracy of AT collected by STH15 has given in [27]. It is a method which based on Statistics. They count the ATE corresponding to every possible SR which will be given a brief introduction in the related work. This is a method based on statistics analysis. But in practical application, it often lack the ability of generalization [26]. We draw the corresponding relationship between SR and ATE according to their statistical results as Fig. 1 shows.

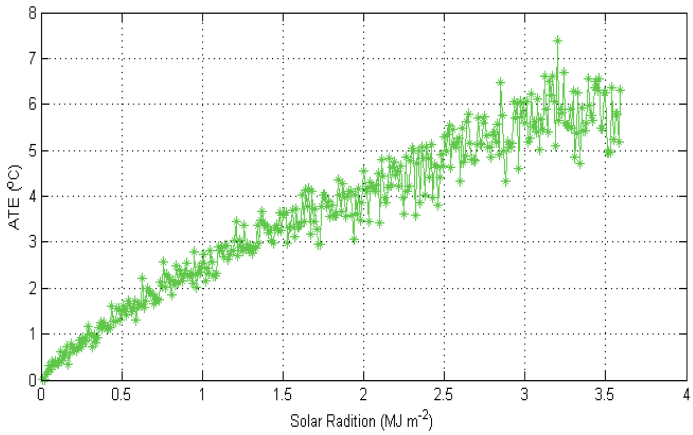

Fig. 1. ATE values corresponding to SR.

As is shown in Fig. 1, it illustrates the relationship between SR and ATE according to the results of [27], each SR corresponds to a unique ATE. Here, the ATE was collected by calculating the average ATE corresponding to every possible value of SR in May. Obviously we can see that, with the rise of SR intensity, ATE also showed an upward trend. But the problem is that, the fluctuation of ATE is too big. Although the difference between the values of the two SR is only 0.1, the statistics of the ATE will be a lot of difference. So, while in the process of correction, it may be cause a relatively large error. And Fig. 2 shows the performance in [27]. We can find that even if the original data curve

of NodeAT is relatively smooth, the volatility of the results after the correction is still great. If we can find a function and a smooth curve to denote the trend of the change of ATE corresponding to SR, it will get a better result.

The BP neural network [10,32] is one of the most widely used neural network models. It can learn and store a large amount of input-output models mapping relationship. Neural networks can be used to do classification [8], clustering [31], prediction [30], etc. In this paper, we use the same data sets in [27] and use BP neural network to build the relationship between ATE and SR due to its powerful ability of non-linear fitting [19]. Finally, we correct the ATE successfully and the experimental results show that our method can find a better relationship between ATE and SR than the method of statistics.

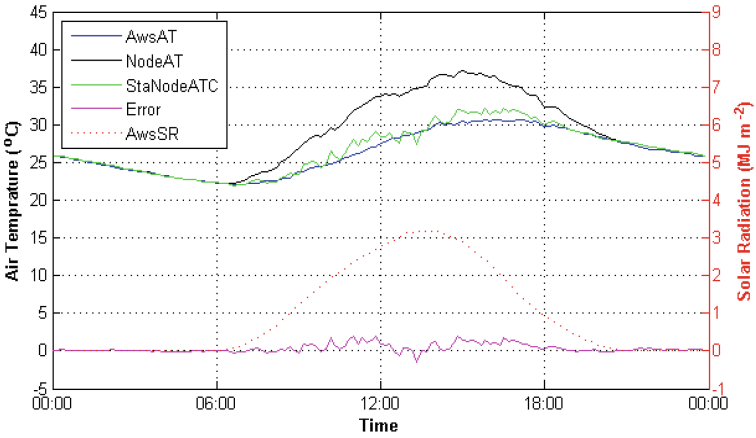

Fig. 2. Correction results using statistical analysis.

2 Proposed Approach

In this paper, we propose BATC, a BP neural network based Air Temperature Correction. The framework of is depicted in Fig. 3. There are four key steps in our framework: (1) Use interpolation method to add sample data. (2) The process of time translation is used to adjust the time coordinate to eliminate the sensing delay between specialized sensors and node sensors. (3) Set up BP neural network model and train it. (4) Use the trained model to calculate the ATE that should be corrected corresponding to SR and then correct the NodeAT.

2.1 Interpolation

First of all, we need to do interpolation with the original data because the sampling frequencies of NodeAT, AwsAT and AwsSR is different. The sampling

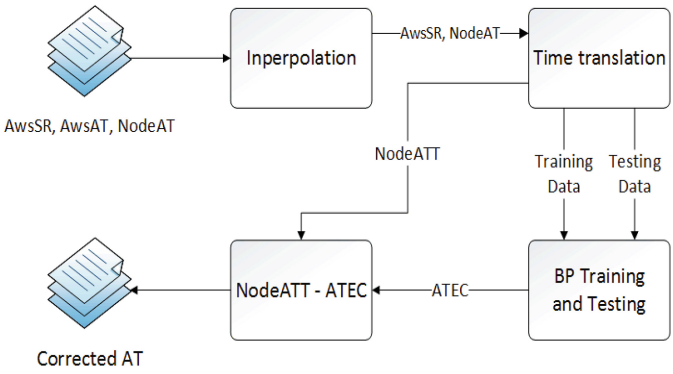

Fig. 3. The framework of data processing and correction.

frequencies of AwsAT, NodeAT and AwsSR is once per minute, once every three minutes and once per hour respectively. As we mentioned in the related work, we select cubic spline interpolation in this paper. We use the interpolation of NodeAT as an example.

Now, a set of raw data of NodeAT has been given as $(nodett_i, nodeAT_i)$, i = 0, 1, 2, ..., n, $nodett_0 < nodett_1 < nodett_2 ... < nodett_n$, interpolation involves the estimation of values of $nodeAT = f(nodett)$ at points $nodett$ in the interval $(nodett_0, nodett_n)$. Cubic spline interpolation can create a piecewise continuous curve passing through each value in the former data set. On each subinterval $(nodett_i, nodett_{i+1})$, we use spline function $S(x)$ to deal with the data to get an intermediate value that we want, where $nodett_i < x < nodett_{i+1}$. People interesting in the detailed information about the cubic spline interpolation algorithm are suggested to refer to paper [11]. In this paper, all the interpolation frequency of NodeAT, AwsAT and AwsSR are once every three minutes according to the sampling frequencies of AwsAT, NodeAT and AwsSR.

2.2 Time Translation

In our WSNs, we need to package for the low-cost sensor SHT15. In order to minimize the cost of our sensing node, the packaging materials we used is also cheap and unprofessional. The temperature of the packing shell can not be kept the same as the actual air temperature at the same time. We know that the temperature of an object which exposed in the air is the same as the temperature of air. When air temperature changes, the temperature of the object will change too with the change of temperature, but due to different specific heat capacity [25] of different materials, the change rate of the temperature will be different. And the thermal conductivity of our unprofessional packaging materials is not very good, it will cause a sensing delay between NodeAT and the actual AT. In addition, the earth and the packing shell will distribute long-wave radiation [6] to the air, these long-wave radiation will affect the sensor too, and these radiation

will continue for some time. However, the sensors in AWS do not suffer from long-wave radiation. So, it is necessary to transform the time coordinate of NodeAT and AwsSR.

2.3 BP Neural Network Modeling

BP neural network is usually optimized through a learning method based on the type of mathematics and statistics. It is a kind of multilayer forward neural network based on error back propagation algorithm. It has the ability to learn and the training methods is supervised. It consists of an input layer, one or more hidden layers and one output layer. When the forward propagation, the direction of propagation is the input layer, the hidden layer, the output layer, the state of each layer of neurons only affects the neurons next layer of next layer. If the output layer can not get the desired output, then the reverse propagation process of the error signal is turned. Through the alternation of the two processes, in the right vector space execution error function gradient descent strategy, dynamic iterative search weight vector, the network error function achieves the minimum value, so as to complete the process of information extraction and the memory.

Hecht-Nielsen demonstrated a feed forward neural network which has three layer with one hidden layer can approximate any multivariate polynomial function [9]. Therefore, we use the three layer BP neural network to establish the model. The topological structure of BP neural network used in this paper is shown in Fig. 4.

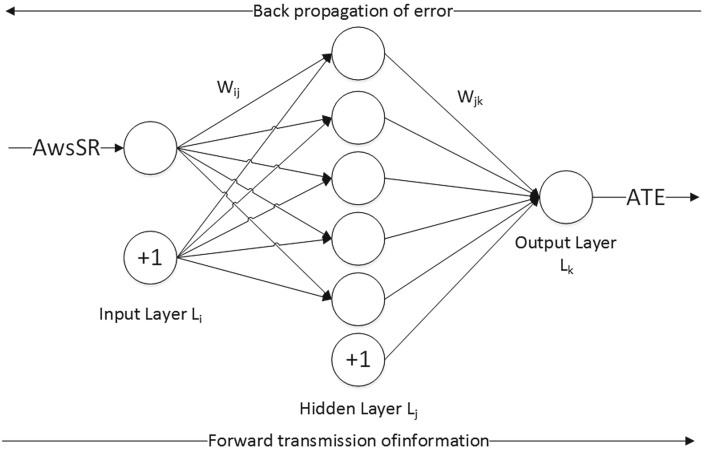

Fig. 4. The framework of data processing and correction.

Where we use $AwsSR$ ($AwsSR = [sr_0, sr_1, \cdots, sr_n]^T$) as the input value of BP neural network and ATE ($ATE = [ate_0, ate_1, \cdots, ate_n]^T$) as the predicted

value of BP neural network. And w_{ij} and w_{jk} are the weights of BP neural network. The circle marked with '+1' is called a bias node. From Fig. 4 we can see that BP neural network can be regarded as a non-linear function. The input and output of BP neural network can seen as the independent variables and dependent variables of the function respectively. When the number of input nodes is n, the number of output nodes is m, the BP neural network is expressed the function mapping relationship from the n independent variables to the m dependent variables. The training steps of BP neural network include the following steps:

Step 1: Network initialization. Determines the network input layer node number$n$, hidden layer node number l, output layer node number m according to the input and output sequence $(AwsSR, ATE)$. Then randomly initialize the connection weights w_{ij} and w_{jk} between input layer, hidden layer and output layer. Then initialize the threshold b in hidden layer and the threshold a in output layer.

Step 2: Calculate the output H of the hidden layer nodes.

$$H_i = f\left(\sum_{i=1}^{n} w_{ij}x_i - a_j\right) \quad j = 1, 2, \cdots, l \tag{1}$$

where l is the node numbers in hidden layer. f is a kind of activation function and the function has many forms of expression. In order to map the data of AwsSR to a range of 0 to 1, we use sigmoid function as the activation function in this paper.

$$f(x) = \frac{1}{1 + e^{-x}} \tag{2}$$

Step 3: Calculate the output O of the output layer nodes according to H, w_{jk} and threshold b.

$$O_k = \sum_{j=1}^{l} H_j w_{jk} - b_k \quad k = 1, 2, \cdots, m \tag{3}$$

Step 4: Calculate the error e of the network according to predicted output O expected output ATE.

$$e = ATE_i - O_i \quad i = 1, 2, \cdots, m \tag{4}$$

Step 5: Update the weights w_{ij} and w_{jk} according to e.

$$w_{ij} = w_{ij} + \eta H_j (1 - H_j) x(i) \sum_{k=1}^{m} w_{jk} e_k \quad j = 1, 2, \cdots, n; k = 1, 2, \cdots, m \tag{5}$$

$$w_{jk} = w_{jk} + \eta H_j e_k \quad j = 1, 2, \cdots, l; k = 1, 2, \cdots, m \tag{6}$$

where η represent the learning rate of BP neural network.

Step 6: Update the threshold b and a according to e.

$$a_j = a_j + \eta H_j \left(1 - H_j\right) \sum_{k=1}^{m} w_{jk} e_k \quad j = 1, 2, \cdots, l \tag{7}$$

$$b_k = b_k + e_k \quad k = 1, 2, \cdots, m \tag{8}$$

Step 7: Determine whether the algorithm achieve the maximum number of iterations or meet the accuracy requirements. If not, turn back to step 2.

This is the whole training process of the BP neural network. After the training of the BP neural network, is means that we have established the relationship between AwsSR and ATE. While in the process of testing, we use AwsSR values corresponding to the NodeAT values as the input of the BP neural network to predict the errors that needed to be corrected. Then use the nodeAT values after the translation process to subtract the errors that needs to be corrected to obtain the corrected NodeAT.

3 Results and Discussion

3.1 Data Collection

The standard data of air temperature and solar radiation used in this research are collected from the AWS at Nanjing University of Information Science and Technology (NUIST). All the measured data also follow the World Meteorological Organization (WMO) requirements. Figure 5a shows a picture of pyranometer in AWS used to collected AwsSR. Figure 5b illustrates the temperature sensor in AWS used to collect AwsAT. Professional temperature sensor is placed in the thermometer screen to prevent the influence of direct radiation of sun and ground radiation, the thermometer screen is horizontally fixed on a special bracket and the height is about 125 cm.

(a) (b)

Fig. 5. Pyranometer and temperature sensor in AWS at UNIST. (a) Temperature sensor (HMP45D) in thermometer screen; (b) The pyranometer in AWS.

Figure 6 shows the our own designed low-cost node that we used in meteorological WSNs. There are four interfaces in the bottom of the node. They are

Fig. 6. Sensing node used in meteorological WSNs. (a) Interfaces on the bottom and solar cell panel in the shell. (b) On-board sensor SHT15 integrated on a circuit board.

used to connect with other meteorological sensors. So it is convenient for us to collect other meteorological factors.

The low-cost sensing node used in the experiment is placed in the vicinity of AWS as Fig. 7 shows. So it is close to the pyranometer which is used to monitor the SR. So we can treat solar radiation collected by AWS as the same as that from which the node suffered.

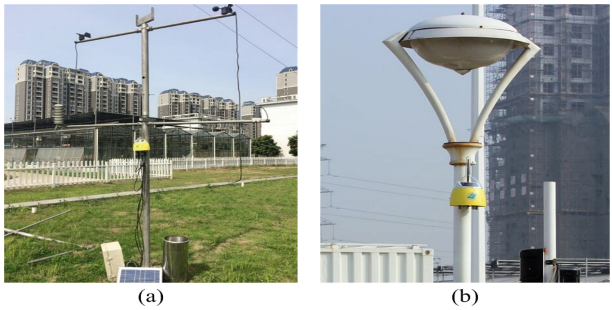

Fig. 7. Placement of sensor nodes. (a) A sensing node with several external meteorological sensors. (b) A sensing node without external sensor connections.

We focus on the same data set in [27] to evaluate the method for error correction in this paper. The data set consists of 8-month meteorological data from 1 May 2014 to 31 December 2014 including NodeAT, AwsAT, battery voltage of node and air humidity at Nanjing University of Information Science and Technology using WSNs and AWS with different kinds of sensors.

3.2 Performance of Time Translation

As is illustrated in Fig. 5, it shows the data of NodeAT, AwsSR and AwsAT before the process of time translation on 3 May 2014. These are the data we randomly selected used to illustrate the process of time translation.

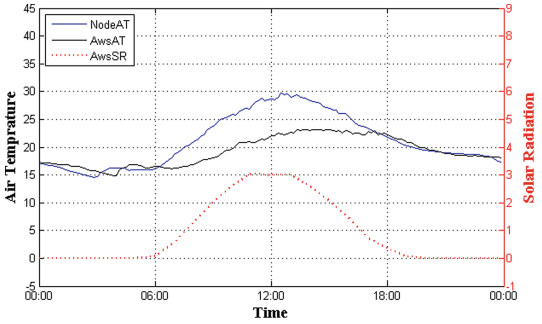

Fig. 8. NodeAT, AwsSR and AwsAT data before the process of time translation on 3 May 2014.

From Fig. 8 we can see that the value of AwsSR is zero in the evening. But theoretically, when the SR is zero, the NodeAT should be essentially consistent with the AwsAT. However, there is still a certain error between NodeAT and AwsAT even in the night. The reason for this phenomenon has been explained in some detail in Sect. 3. In order to eliminate the delay between the professional and the unprofessional sensors, we finally translate NodeAT and AwsSR to the future by 60 min. We can see the performance in Fig. 9.

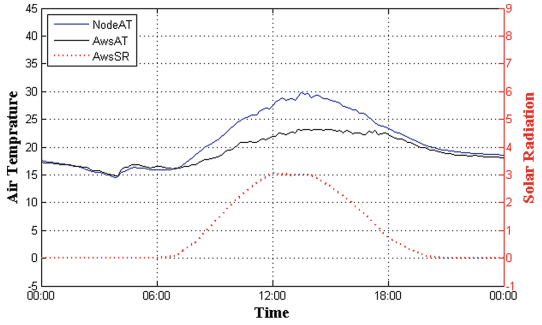

Fig. 9. NodeAT, AwsSR and AwsAT data after the process of time translation on 3 May 2014.

According to experimental result shows that when the translation time is 60 min, the performance gets to the best.

3.3 Performance Contrast of BP Neural Network and Statistical Analysis

In this experiment, we report the performance of the BP neural network model in Fig. 4 as this model achieve the best performance. This architecture is denoted

as BP^s_{151} since the input parameter is only AwsSR (the superscript s) and the node numbers in each layer are 1, 5, 1 (the subscript 151). Here, the bias nodes not included. The number of nodes in the hidden layer is generally determined by the following formula:

$$q = \sqrt{n+m} + a \tag{9}$$

where n is the input node number, m is the output node number, a is the constant between 1 to 10. According to the experimental results, we determine the optimal number of hidden layer nodes is 5 (bias node not included). We put the prediction results of BP^s_{151} and the results obtained by the statistical method in Fig. 9.

From Fig. 9 we can see that the blue curve is the prediction value of BP^s_{151}, it is a smooth curve. So there will not be much volatility when using this curve to correct the ATE values (Fig. 10).

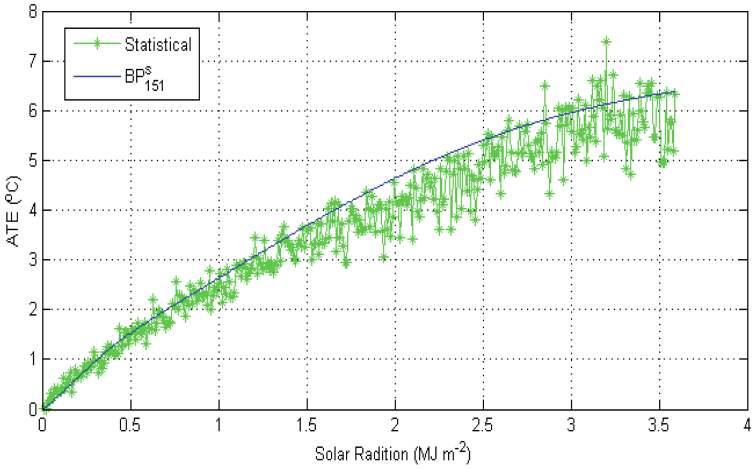

Fig. 10. ATE values corresponding to every possible value of SR.

3.4 Performance Evaluations

In order to show the superiority of our method numerically, we got the results in [27] and focus on the maximum absolute error, the mean absolute error and the standard deviation of the data to illustrate it. In addition, we use the formula (10) to calculate the correction efficiency in Tables 1, 2 and 3.

$$Efficiency = \frac{rawData - errorCorrected}{rawData} * 100\,\% \tag{10}$$

In Table 1, we took two days of data per month from June to December to calculate their maximum absolute errors respectively. Raw data represents the

Table 1. Maximal absolute error in different correcting phases.

	Maximal absolute error			
Date	Raw data	Time translation	Error corrected	Efficiency
2014.06.04	7.55	5.96	1.87	75 %
2014.06.09	8.06	6.75	1.00	87 %
2014.07.04	2.76	2.26	0.56	80 %
2014.07.07	8.53	7.17	2.83	67 %
2014.08.08	2.03	1.35	0.57	72 %
2014.08.10	7.06	6.26	1.65	77 %
2014.09.03	6.10	4.80	1.65	73 %
2014.09.28	8.44	7.26	2.14	75 %
2014.10.02	5.84	4.56	1.10	81 %
2014.10.19	8.56	6.76	2.35	73 %
2014.11.11	7.10	4.66	2.46	65 %
2014.11.22	7.97	6.87	2.98	63 %
2014.12.07	6.21	5.23	1.16	81 %
2014.12.21	5.79	5.09	1.83	68 %
Average	**6.57**	**5.36**	**1.73**	**74 %**
Results in [27]	6.61	5.44	2.24	66 %

Table 2. Mean absolute error in different correcting phases.

	Mean absolute error			
Date	Raw data	Time translation	Error corrected	Efficiency
2014.06.04	2.78	2.22	0.48	83 %
2014.06.09	2.82	2.35	0.26	91 %
2014.07.04	0.73	0.65	0.16	78 %
2014.07.07	2.89	2.55	0.68	76 %
2014.08.08	0.68	0.63	0.28	59 %
2014.08.10	2.08	1.83	0.37	82 %
2014.09.03	1.62	1.54	0.33	80 %
2014.09.28	2.41	2.08	0.55	77 %
2014.10.02	1.87	1.45	0.31	83 %
2014.10.19	2.17	1.78	0.45	79 %
2014.11.11	1.83	1.50	0.61	67 %
2014.11.22	1.98	1.60	0.59	70 %
2014.12.07	1.96	1.39	0.44	78 %
2014.12.21	1.81	1.41	0.56	69 %
Average	**1.97**	**1.64**	**0.43**	**77 %**
Results in [27]	1.96	1.58	0.50	74 %

Table 3. Standard deviation in different correcting phases.

Date	Standard deviation			
	Raw data	Time translation	Error corrected	Efficiency
2014.06.04	3.06	2.31	0.57	81 %
2014.06.09	3.24	2.53	0.31	90 %
2014.07.04	0.91	0.66	0.19	79 %
2014.07.07	3.11	2.61	0.84	73 %
2014.08.08	0.49	0.32	0.22	55 %
2014.08.10	2.45	1.98	0.30	88 %
2014.09.03	1.93	1.52	0.45	77 %
2014.09.28	3.22	2.48	0.56	83 %
2014.10.02	2.09	1.51	0.34	84 %
2014.10.19	2.77	2.09	0.55	80 %
2014.11.11	2.25	1.57	0.67	70 %
2014.11.22	2.80	2.24	0.86	69 %
2014.12.07	2.65	1.94	0.65	75 %
2014.12.21	2.32	1.86	0.72	69 %
Average	**2.38**	**1.83**	**0.52**	**77 %**
Results in [27]	2.38	1.82	0.62	74 %

data without treatment and it can be seen that the error is the biggest. After the process of time translation, the error values were reduced by a small margin. The third column shows the maximum absolute error between the corrected data and the standard data with BP^{s}_{151}. This process greatly reduces the error. After the correction, our average maximal absolute error is 0.51 lower than that of them and the efficiency is improved by 8 % compared with the results in [27].

In Table 2, we calculated the mean absolute error of these days. Similarly, the errors gradually decreased with the process of time translation and correction. After the errors were corrected, our average maximal absolute error is 0.07 lower than that of them and the efficiency is improved by 3 % compared with the results in [27].

In Table 3, we calculated the error between the corrected data and the standard data. The greater the standard deviation, the greater the volatility. After the errors were corrected, our average maximal absolute error is 0.1 lower than that of them and the efficiency is improved by 3 % compared with the results in [27].

Comparing the average results and efficiency after error correction through these three indicators, we can find that our results are superior to the result in previous paper.

4 Conclusions

We use BP neural networks for error correction in this paper. We analyzed the data collected from the automatic weather station and wireless sensor network and did some pretreatments, and successfully fitted the function relationship between SR and ATE. We evaluated the performs of this model and finally corrected the errors. Experiment results show that the corrected data performs very well and the data of maximum absolute error, mean absolute error and standard deviation are all get reduced comparing with the performance of the method of statistical analysis, demonstrating its superior in ATE correction.

However, the cost of SR sensing is still very high. So in the future, we will study the relationship between the solar cell panel voltage and SR and then convert the voltage to the corresponding SR. If this method can be successful, we can use the voltage to replace the SR so that our correction will become more economical.

Acknowledgements. This work is supported by the National Science Foundation of China under Grant No. 61173136, U1536206, 61232016, U1405254, 61373133, 61502242, the CICAEET (Jiangsu Collaborative Innovation Center on Atmospheric Environment and Equipment Technology) fund and PAPD (Priority Academic Program Development of Jiangsu Higher Education Institutions) fund.

References

1. Arakawa, M., Okamoto, K., Yi, K., Terabayashi, M., Tsutsumi, Y.: Shrimp U-Pb dating of zircons related to the partial melting in a deep subduction zone: case study from the sanbagawa quartz-bearing eclogite. I. Arc **22**(1), 74–88 (2011)
2. Barroca, N., Borges, L.M., Velez, F.J., Monteiro, F., Grski, M., Castro-Gomes, J.: Wireless sensor networks for temperature and humidity monitoring within concrete structures. Constr. Build. Mater. **40**(3), 1156–1166 (2013)
3. Bojanowski, J.S., Vrieling, A., Skidmore, A.K.: A comparison of data sources for creating a long-term time series of daily gridded solar radiation for Europe. Sol. Energy **99**(1), 152–171 (2014)
4. Box, J.E., Rinke, A.: Evaluation of Greenland ice sheet surface climate in the HIRHAM regional climate model using automatic weather station data. J. Clim. **16**(9), 1302–1319 (2003)
5. Elfelly, N., Dieulot, J.Y., Benrejeb, M., Borne, P.: A multimodel approach of complex systems identification and control using neural and fuzzy clustering algorithms. In: International Conference on Machine Learning Applications, pp. 93–98 (2010)
6. Flerchinger, G.N., Xaio, W., Marks, D., Sauer, T.J., Yu, Q.: Comparison of algorithms for incoming atmospheric long-wave radiation. Water Resour. Res. **45**(3), 450–455 (2009)
7. Fu, X.: Test and analysis of temperature characteristics for HMP45D humidity sensors. Meteorol. Sci. Technol. (2009)
8. Gu, B., Sheng, V.S., Wang, Z., Ho, D., Osman, S., Li, S.: Incremental learning for v-support vector regression. Neural Net. Official J. Int. Neural Net. Soc. **67**(C), 140–150 (2015)

9. Hecht-Nielsen, R.: Theory of the backpropagation neural network. Neural Netw. **1**(1), 65–93 (1988)
10. Huang, G.B., Zhu, Q.Y., Siew, C.K.: Extreme learning machine: theory and applications. Neurocomputing **70**(13), 489–501 (2006)
11. Interpolation, C.S.: Cubic spline interpolation. Numer. Math. J. Chinese Univ. **64**(1), 44–56 (1999)
12. Izadi, D., Abawajy, J.H., Ghanavati, S., Herawan, T.: A data fusion method in wireless sensor networks. Sensors **15**(2), 2964–2979 (2015)
13. Jin, M.: Analysis and verification of HMP45D humidity sensor fault in dalian airport. Wireless Internet Technol. (2015)
14. Jing, Z., Jun, L.I., Schmit, T.J., Jinlong, L.I., Liu, Z.: The impact of airs atmospheric temperature and moisture profiles on hurricane forecasts: Ike (2008) and Irene (2011). Nat. Cell Biol. **32**(3), 966–972 (2015)
15. Kadar, I.: Perceptual reasoning in adaptive fusion processing. Proc. SPIE Int. Soc. Opt. Eng. **69**(1), 168–180 (2002)
16. Liu, H., Wang, B., Sun, X., Li, T., Liu, Q., Guo, Y.: DCSCS: a novel approach to improve data accuracy for low cost meteorological sensor networks. Inf. Technol. J. **13**(9), 1640–1647 (2014)
17. Liu, X., Cheng, X., Skidmore, A.K.: Potential solar radiation pattern in relation to the monthly distribution of giant pandas in foping nature reserve, China. Ecol. Model. **222**(3), 645–652 (2011). (online first)
18. Miller, F.P., Vandome, A.F., Mcbrewster, J.: Automatic weather station. Bioscience **196**(3366), 321–321 (2010)
19. Moroni, G., Syam, W.P., Petr, S.: Performance improvement for optimization of the non-linear geometric fitting problem in manufacturing metrology. Measur. Sci. Technol. **25**(8), 1409–1424 (2014)
20. Perez, P., Vermaak, J., Blake, A.: Data fusion for visual tracking with particles. Proc. IEEE **92**(3), 495–513 (2004)
21. Guo, P., Jin Wang, B.L., Lee, S.: A variable threshold-value authentication architecture for wireless mesh networks. J. Internet Technol. **15**(6), 929–935 (2014)
22. Prakash, D., Mageshwari, T.U., Prabakaran, K., Suguna, A.: Detection of heart diseases by mathematical artificial intelligence algorithm using phonocardiogram signals. Int. J. Innov. Appl. Stud. **3**(1), 145–150 (2013)
23. Roweis, S.T., Saul, L.K.: Nonlinear dimensionality reduction by locally linear embedding. Science **290**(5500), 2323–6 (2000)
24. Shen, J., Tan, H., Wang, J., Wang, J., Lee, S.: A novel routing protocol providing good transmission reliability in underwater sensor networks. J. Internet Technol. **16**(1), 171–178 (2015)
25. Sin, L.T., Rahman, W.A.W.A., Rahmat, A.R., Morad, N.A., Salleh, M.S.N.: A study of specific heat capacity functions of polyvinyl alcoholcassava starch blends. FEBS Lett. **31**(1–3), 3137 (2010)
26. Steiniger, S., Taillandier, P., Weibel, R.: Utilising urban context recognition and machine learning to improve the generalisation of buildings. Int. J. Geogr. Inf. Sci. **24**(24), 253–282 (2010)
27. Sun, X., Yan, S., Wang, B., Li, X., Liu, Q., Zhang, H.: Air temperature error correction based on solar radiation in an economical meteorological wireless sensor network. Sensors **15**(8), 18114–39 (2015)
28. Trontz, A., Cheng, B., Zeng, S., Xiao, H., Dong, J.: Development of metal-ceramic coaxial cable Fabry-Perot interferometric sensors for high temperature monitoring. Sensors **15**(10), 24914–24925 (2015)

29. Xie, S., Wang, Y.: Construction of tree network with limited delivery latency in homogeneous wireless sensor networks. Wireless Pers. Commun. **78**(78), 231–246 (2014)
30. Zhang, Y., Gao, X., Katayama, S.: Weld appearance prediction with BP neural network improved by genetic algorithm during disk laser welding. J. Manuf. Syst. **34**, 53–59 (2015)
31. Zheng, Y., Byeungwoo, J., Xu, D., Wu, Q.M.J., Zhang, H.: Image segmentation by generalized hierarchical fuzzy c-means algorithm. J. Intell. Fuzzy Syst. **28**(2), 4024–4028 (2015)
32. Zipser, D., Andersen, R.A.: A back-propagation programmed network that simulates response properties of a subset of posterior parietal neurons. Nature **331**(6158), 679–684 (1988)